

Stiffness matters: Improved failure risk assessment of ascending thoracic aortic aneurysms



Klaas Vander Linden, MSc,^a Emma Vanderveken, PhD,^b Lucas Van Hoof, MD,^c Lauranne Maes, PhD,^a Heleen Fehervary, PhD,^{a,d} Silke Dreesen, MSc,^a Amber Hendrickx, MSc,^b Peter Verbrugge, PhD,^c Filip Rega, PhD,^c Bart Meuris, PhD,^c and Nele Famaey, PhD^{a,d}

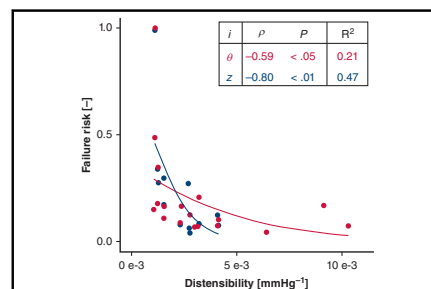
ABSTRACT

Objectives: Rupture and dissection are feared complications of ascending thoracic aortic aneurysms caused by mechanical failure of the wall. The current method of using the aortic diameter to predict the risk of wall failure and to determine the need for surgical resection lacks accuracy. Therefore, this study aims to identify reliable and clinically measurable predictors for aneurysm rupture or dissection by performing a personalized failure risk analysis, including clinical, geometrical, histologic, and mechanical data.

Methods: The study cohort consisted of 33 patients diagnosed with ascending aortic aneurysms without genetic syndromes. Uniaxial tensile tests until failure were performed to determine the wall strength. Material parameters were fitted against ex vivo planar biaxial data and in vivo pressure–diameter relationships at diastole and systole, which were derived from multiphasic computed tomography (CT) scans. Using the resulting material properties and in vivo data, the maximal in vivo stress at systole was calculated, assuming a thin-walled axisymmetric geometry. The retrospective failure risk was calculated by comparing the peak wall stress at suprasystolic pressure with the wall strength.

Results: The distensibility coefficient, reflecting aortic compliance and derived from blood pressure measurements and multiphasic CT scans, outperformed predictors solely based on geometrical features in assessing the risk of aneurysm failure.

Conclusions: In a clinical setting, multiphasic CT scans followed by the calculation of the distensibility coefficient are of added benefit in patient-specific, clinical decision-making. The distensibility derived from the aneurysm volume change has the best predictive power, as it also takes the axial stretch into account. (JTCVS Open 2023;16:66–83)



Aneurysm failure risk in function of the distensibility.

CENTRAL MESSAGE

The distensibility, ie, the capacity of the vessel to expand during pressure changes, outperforms purely geometrical predictors when assessing the failure risk of ascending thoracic aortic aneurysms.

PERSPECTIVE

The distensibility outperforms purely geometrical predictors when assessing the failure risk of ascending thoracic aortic aneurysms. The aneurysm should be visualized at 2 phases, ie, at diastole and systole. Clinicians can add this metric to the risk stratification process, where it can gradually replace purely geometrical predictors as the database and confidence in a cut-off value grows.

From the Departments of ^aMechanical Engineering and ^bCardiovascular Sciences, KU Leuven; ^cDepartment of Cardiac Surgery, University Hospitals Leuven; and ^dFIBer, KU Leuven Core Facility for Biomechanical Experimentation, Leuven, Belgium.

The authors thank Research Foundation–Flanders (FWO) (grant nos.: SB1SA9119N, SB1S56317) and KU Leuven (C2-ADAPT) for providing financial support to this project.

Drs Meuris and Famaey are joint last authors.

Received for publication May 24, 2023; revisions received Sept 7, 2023; accepted for publication Sept 11, 2023; available ahead of print Oct 17, 2023.

Address for reprints: Nele Famaey, PhD, Department of Mechanical Engineering, KU Leuven, Celestijnenlaan 300 - Box 2419, 3001 Leuven, Belgium (E-mail: nele.famaey@kuleuven.be).

2666-2736

Copyright © 2023 The Author(s). Published by Elsevier Inc. on behalf of The American Association for Thoracic Surgery. This is an open access article under the CC BY-NC-ND license (<http://creativecommons.org/licenses/by-nc-nd/4.0/>). <https://doi.org/10.1016/j.xjon.2023.09.008>

Abbreviations and Acronyms

AHI	= aortic height index
ASI	= aortic size index
ATAA	= ascending thoracic aortic aneurysm
DC	= distensibility coefficient
DFR	= deterministic failure risk

An ascending thoracic aortic aneurysm (ATAA) is a chronic degenerative disease characterized by a permanent dilation of the aortic wall, which can culminate in a life-threatening emergency when the wall ruptures or dissects.¹ In theory, prophylactic replacement of the aorta should be performed when the risk of rupture or dissection is greater than the interventional risk. In clinical practice, the rupture or dissection risk is assessed by geometric factors. Currently, surgical repair is recommended when the maximum aortic diameter exceeds the threshold value of 55 mm, or when the growth exceeds 5 mm per year.² The mentioned values may vary in case other risk factors are present, such as a bicuspid aortic valve, genetic syndromes (Marfan, Loeys–Dietz and Turner syndrome), hypertension, and family history of dissection.³ Research has shown that the diameter criterion poorly represents the individual risk, resulting in a large number of false positives and false negatives.^{4,5}

In search of better predictive tools to assess the failure risk, some have indicated that the diameter should be indexed by patient body surface area (aortic size index, ASI)⁶ or height (aortic height index, AHI).⁷ Others have pointed out that the axial length of the ATAA, measured as the distance between the annulus and the brachiocephalic artery, may improve the risk stratification.⁸

Essentially, wall failure is a biomechanical phenomenon, since it occurs when the load, ie, wall stress or strain, exerted on the aortic wall exceeds its load-bearing capacity, ie, wall strength or extensibility.⁹ Therefore, biomechanical models to predict failure risk have gained increasing attention. Martin and colleagues¹⁰ compared aortic wall stiffness with the risk of rupture. Although a decreased compliance seemed to correlate with an increased risk, one major limitation of this study was that the authors neglected the in vivo wall thickness when calculating the risk, so there was no compelling evidence of the wall stiffness' risk potential.

Despite these findings, recent publications demonstrate that the ongoing clinical debate is still primarily dominated by the diameter criterion.^{11,12} There is need for clear evidence and more reliable guidelines to identify patients at risk of aneurysm rupture or dissection. To identify reliable and clinically measurable predictors, we performed a retrospective personalized failure risk analysis, including clinical, geometrical, histologic, and mechanical data from patients undergoing surgery for an ATAA.

METHODS

The study was approved by the Ethics Committee Research UZ/KU Leuven (NCT03142074, approved on December 23, 2016) and patient informed consent for publication of study data was obtained. The cohort consisted of 33 adult patients who underwent surgery at the University Hospitals Leuven. Patients were included if they had an ascending aortic diameter larger than 55 mm, or 50 mm in case of aortic valve issues such as aortic valve stenosis or aortic insufficiency, as measured by the surgeons within the clinical routine, following the guidelines presented in Iselbacher and colleagues,² or if they underwent resection of the ascending aorta during the Ross procedure. Patients with genetic syndromes such as Marfan, Loeys–Dietz, and Turner were excluded from the study. Before surgery, patients underwent an electrocardiogram-gated contrast-enhanced computed tomography scan and the diastolic (p_{dias}) and systolic (p_{sys}) pressures were measured noninvasively. All patients were operated under cardiopulmonary bypass with arrested heart via sternotomy. The ascending aorta was excised and sent for further analysis.

Histologic Analysis

Samples for histologic analysis were fixed in paraformaldehyde (6%), dehydrated (Mediate TES 99), and embedded in paraffin. Then, 5- μ m-thick serial cross-sections were created (Microm HM360) and stained with hematoxylin and eosin and Elastica van Gieson stains using standard laboratory protocols. All specimens were microscopically examined (Philips Ultra Fast Scanner). The thickness of the entire wall and sublayers, ie, intima, media, and adventitia, was calculated as the average at 10 different locations of the slice with ImageJ 1.52a (National Institutes of Health). The fractions of the wall constituents, ie, elastin, collagen, and smooth muscle cells, were measured using an in-house developed image processing software written in MATLAB R2023a (MathWorks Inc). The presence of intimal hyperplasia and medial degeneration (moderate or severe) was qualitatively assessed according to guidelines presented in Halushka and colleagues.¹³ All measurements and assessments were performed by 2 independent observers.

Geometrical Analysis

Preoperative electrocardiogram-gated computed tomography scans, each consisting of approximately 600 to 800 transversal slices with an in-plane resolution of 0.34 mm and a slice thickness of 0.6 mm, were segmented and reconstructed into a 3-dimensional model at end-diastole ($k=dias$, 0% RR-interval) and mid-systole ($k=sys$, 33% RR-interval) phase using Mimics Innovation Suite 23 (Materialise).¹⁴ At both phases k , the luminal volume of the aorta, was segmented (Figure 1). The maximal diameter D_k was defined by the best-fit circle along the center line at the widest point of the aneurysm. The length of the aneurysm L_k was defined as the distance along the center line between the sinotubular junction and the first bifurcation, ie, the brachiocephalic artery. Consequently, the volume of the aneurysm V_k was defined as the volume of the aorta measured along the center line between the sinotubular junction proximally and the brachiocephalic artery distally. Moreover, AHI was calculated as $AHI = \frac{D_{sys}}{l}$, with l the height of the patient⁷ and the ASI was calculated as $ASI = \frac{D_{sys}}{\sqrt{\frac{bw}{3.6 \times 58 \text{ gm}^{3.5}}}}}$, with w the weight of the patient.¹⁵

Mechanical Analysis

In vivo mechanical characterization. The in vivo distensibility coefficient (DC) defines the vessel compliance and reflects the capacity of the vessel to expand during pressure changes. The DC based on the cross-sectional area is defined as follows¹⁶:

$$DC_A = \frac{D_{sys}^2 - D_{dias}^2}{D_{dias}^2 (p_{sys} - p_{dias})}. \quad (1)$$

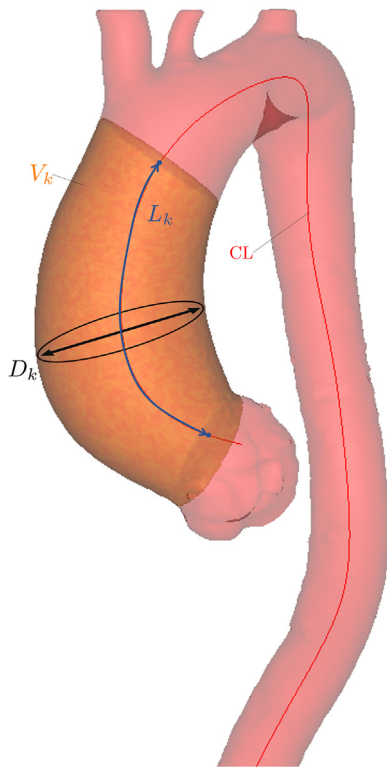


FIGURE 1. Example of a segmented aorta (pink) with the ATAA (orange) and centerline (CL) (red). The aneurysm’s volume (V_k), maximal diameter (D_k), and length (L_k) were measured based on the segmentation at phase $k=dias,sys$.

The previous equation ignores the geometrical changes in axial direction of the ATAA between diastole and systole. Therefore, we define an alternative measure for the DC, based on the volume:

$$DC_V = \frac{V_{sys} - V_{dias}}{V_{dias}(p_{sys} - p_{dias})}. \quad (2)$$

In vitro mechanical characterization. After aortic replacement, the excised tissue intended for mechanical testing was preserved in phosphate-buffered saline solution at -80°C . Experiments were performed at FIBER, KU Leuven Core Facility for Biomechanical Experimentation. After thawing overnight at 4°C , the tissue was cut open axially and the samples, hourglass-shaped for uniaxial or square-shaped for biaxial tensile testing, were excised according to the tissue’s circumferential (θ) and axial (z) direction of the aorta (Figure 2). In some cases, insufficient tissue was available for testing all the indicated samples. Sample thickness was measured with a VHX-6000 Digital Microscope (Keyence Corporation). All tensile tests were performed using a Messphysik testing device (ZwickRoell). Images were captured at 20 Hz with Vic-Snap (Correlated Solutions, with isi-sys as system integrator) using a Manta G-917B camera with a Sony ICX814 monochrome charged-coupled device, mounted perpendicularly to the sample’s surface. The samples were submerged in saline solution at 37°C during mechanical testing. For a detailed description of the test protocols, the reader is referred to Appendix E1.

To estimate the wall strength, hourglass samples were mounted on a uniaxial test set-up using clamps and were loaded until rupture (Figure 3). The

strength of the tissue Y_{ii} in the direction $i=\theta,z$ is expressed in terms of the first Piola–Kirchhoff stress and is calculated as follows:

$$Y_{ii} = \frac{\varphi f_{ii}^y}{W_0 H_0} \quad (3)$$

With f_{ii}^y the normal force measured at yield, defined according to Martin and colleagues,¹⁰ in direction i , and W_0 and H_0 the width and thickness measured at the gauge section in the stress-free state, respectively. $\varphi=1.06$ is the factor that incorporates the stress concentrations arising from the hourglass shape of the test specimen.

To characterize the mechanical behavior, square samples were mounted on a planar biaxial testing set-up using rakes (Figure 3). The samples were cyclically loaded along their circumferential and axial axes. Experimental forces in the circumferential ($f_{\theta\theta}$) and longitudinal direction (f_{zz}) were measured. The corresponding deformation at the center of the sample was measured with digital image correlation.¹⁷

Determining Failure Risk

Calculation of the intraluminal maximal wall stress requires information on the material behavior and in vivo wall thickness of the tissue. The material parameters s and wall thickness at diastole H_{dias} were estimated using a material fitting approach explained in^(18,19), by minimizing the difference between (1) the experimental (f_{ii}) and model (f_{ii}^{mod}) reaction forces in the direction $i=\theta,z$ of the planar biaxial test, (2) the measured (H_0) and model (H_0^{mod}) ex vivo thickness and (3) the measured (p_{sys}) and model (p_{sys}^{mod}) systolic blood pressure (Figure 3). Knowing the material parameters and in vivo thickness, the PWS_{ii} , first Piola–Kirchhoff peak wall stress in the direction i at supra-systolic blood pressure, was calculated while approximating the aneurysm as a thin-walled cylinder. More specifically, the aneurysm at diastole was further pressurized and axially stretched using $110\%p_{sys}$ and $\lambda_{sys,zz} = \frac{L_{sys}}{L_{dias}}$, respectively.

The deterministic failure risk DFR_i in the direction i was calculated as the ratio between the maximal estimated in vivo wall stress and the wall strength: $DFR_i = \frac{PWS_{ii}}{Y_{ii}}$. A low value of DFR_i means that the aneurysm is unlikely to rupture or dissect in the direction i , and vice versa. In addition, to address the uncertainty associated with the input variables used to compute the wall stress, a probabilistic failure risk (PFR_i) was calculated by considering the stochastic nature of the wall thickness and blood pressure. PFR_i values are negative, and as they approach zero, the likelihood of aneurysm failure increases, with zero representing a 100% chance.²⁰ A schematic representation of the deterministic and probabilistic failure risk estimation is shown in Figure 3. For a detailed description of the parameter fitting approach, the maximal in vivo stress and the failure risk estimation, the reader is referred to Appendix E2.

Statistical Analysis

Statistical analysis was performed using RStudio. Comparisons were determined using the Mann–Whitney U test and the Fisher exact test for continuous and categorical variables, respectively. Correlations were determined using the Spearman rank nonparametric test. Simple logistic regression was performed to establish a relationship between DFR_i and possible predictors, linear regression was performed to establish a relationship between PFR_i and possible predictors.

RESULTS

Subject Characteristics

The subject characteristics are summarized in Table 1. The data set was categorized into 2 different groups depending on their area-based distensibility coefficient DC_A in relation to DC_A^{phys} . DC_A^{phys} was set to $1.0e-3 \text{ mm Hg}^{-1}$, representing the third decile of the reported values for the

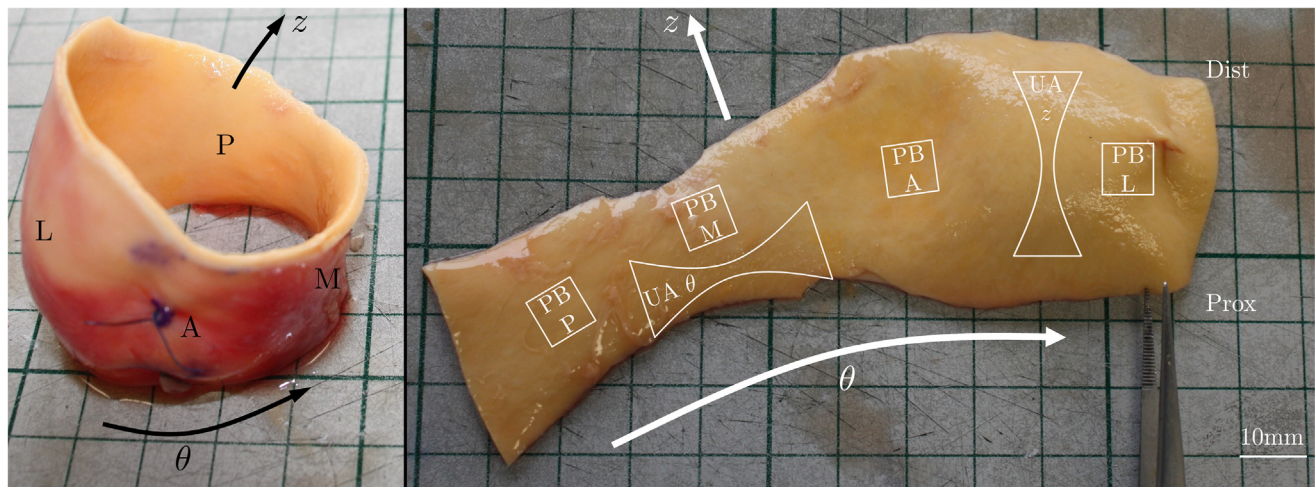


FIGURE 2. Excised, load-free (*left*) and opened, stress-free (*right*) ATAA. Hourglass and square-shaped samples for uniaxial (UA) and planar biaxial (PB) tensile testing are indicated, respectively, as well as the proximal (*prox*) and distal (*dist*) side, and the axial (z) and circumferential (θ) direction. PB samples were extracted from the 4 quadrants (A, anterior; M, medial or inner curvature; P, posterior; L, lateral or outer curvature). ATAA, Ascending thoracic aortic aneurysm.

healthy population's ascending aortic distensibility.²² If $DC_A \leq DC_A^{phys}$, the aneurysm was classified as “stiff,” if $DC_A > DC_A^{phys}$, the aneurysm was classified as “compliant”.

Figure 4 shows the volume-based distensibility in function of the patient's age. The fitted material parameters s and diastolic wall thickness H_{dias} of each patient, together with the fitting measures are shown in Appendix E3, Table E2.

Failure Risk Assessment

Table 2 presents the Spearman ρ correlation coefficients with corresponding P values between the different clinically accessible characteristics and the failure risk DFR_i ($i=\theta, z$). Figure 5 shows the failure risk DFR_i ($i=\theta, z$) as function of D_{sys} , AHI , DC_A , and DC_V . The Spearman ρ correlation coefficient with corresponding P value and Nagelkerke pseudo R^2 value of the logistic regression is also shown in the figure. All but 1 aneurysm was predicted not to rupture or dissect, ie, $DFR_i < 1$ ($i=\theta, z$). For the one aneurysm for which $DFR_{\theta\theta}$ and $DFR_{zz}=1.10$, the failure risk was retrospectively set to 1, since no ATAA had ruptured or dissected before surgery. A significant increase of the failure risk in the circumferential direction was observed for hypertensive patients with respect to normotensive patients. No significant difference could be observed for the failure risk between patients with tricuspid and bicuspid aortic valves. The probabilistic failure risk assessment shows the same trends as the deterministic approach, the results of which are described in Appendix E4.

DISCUSSION

We performed a retrospective patient-specific failure risk analysis of ascending thoracic aortic aneurysms, including

clinical, geometrical, histologic, and mechanical data. Uniaxial tensile tests were performed to determine the wall strength and material parameters were fitted against in vitro planar biaxial data and in vivo pressure–diameter relationships at diastole and systole. Using the resulting material properties and in vivo data, the maximal in vivo stress at systole was calculated, assuming a thin-walled axisymmetric geometry. Failure risks were defined by comparing the peak wall stress with the wall strength. The failure risks were compared with clinically accessible predictors to predict aneurysm failure. In addition, age-related changes to the aneurysm behavior and wall morphology were investigated.

Aneurysm Failure Risk Assessment

The presented results in Figure 5 and Table 2 again confirm the inadequacy of the diameter when assessing the failure risk of ATAA.^{4,6} Likewise, alternative geometrical features such as the aneurysm length or volume do not correlate with the failure risk DFR_i , although they are recommended by others.⁸ Although the diameter indexed against the patient height (AHI) slightly improves the risk assessment in the circumferential direction, the AHI and ASI (indexing the diameter against the patient body surface area) do not result in statistically significant correlations in either direction, contrary to what has been suggested in literature.^{6,7} However, hypertension, which has been identified as a risk factor in multiple cardiovascular diseases, does lead to a greater failure risk in the circumferential direction.^{16,23}

As aneurysm rupture or dissection is primarily a mechanical event, mechanical predictors have the possibility to improve the risk stratification. The distensibility coefficient

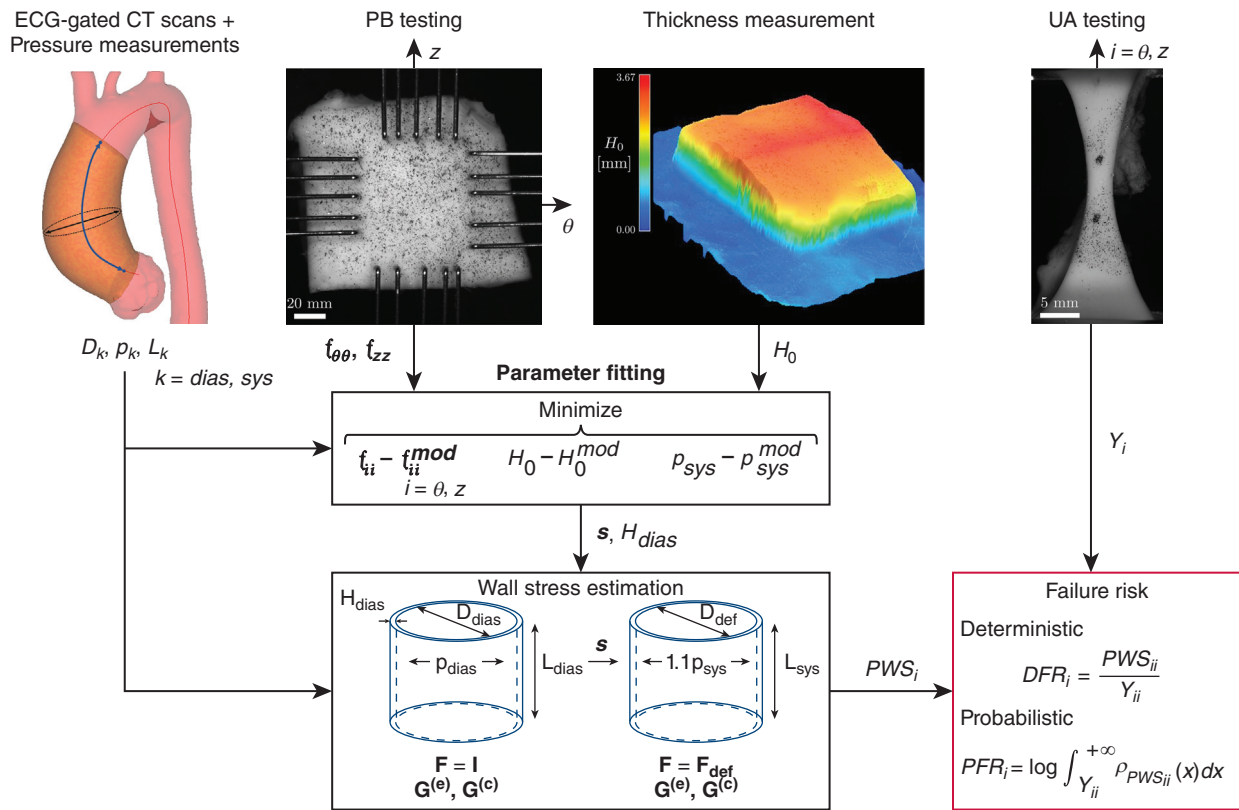


FIGURE 3. Overview of the retrospective personalized failure risk assessment. ECG, Electrocardiogram; CT, computed tomography; PB, planar biaxial; UA, uniaxial; H_0 , ex vivo thickness; p_{sys} , systolic blood pressure; H_{dias} , in vivo wall thickness at diastole; D_{dias} , maximal aortic diameter measured at diastole; p_{dias} , diastolic blood pressure; s , material properties; D_{def} , diameter in the supra-systolic state; DFR_i , deterministic failure risk; PFR_i , probabilistic failure risk.

expresses the ability of the artery to dilate in response to an increase in pressure.¹⁶ The area-based DC expresses the compliance in terms of the diameter and relates it to the corresponding pressure increase. Through the classification of aneurysms according to their distensibility relative to a reference healthy distensibility (as outlined in Table 1), it becomes evident that stiff aneurysms exhibit greater dimensions in terms of axial length, diameter (including derived variables AHI and ASI), and volume compared with compliant aneurysms. Furthermore, this classification enables us to differentiate aneurysms at low risk, associated with high compliance, from those at greater risk, associated with high stiffness. A low distensibility is also associated with weaker tissue in the circumferential direction.

Consequently, the failure risk DFR_i in both circumferential and axial direction exhibits a significant correlation with DC_A . The lower its compliance, the stiffer the material becomes and the greater the failure risk DFR_i . This is in accordance with Martin and colleagues,¹⁰ who defined a similar empirical mechanical coefficient, ie, the (diameter-based) pressure–strain modulus to quantify the stiffness of the aorta and found that this predictor has a strong relation

with the failure risk. In addition to this, Emerel and colleagues²⁴ observed a significant decrease of the distensibility among 7 dissected ATAA cases when compared with 7 nondissected cases, deriving the distensibility from diameter measurements. This was confirmed by a more recent study.²⁵ However, considering the elevated circumferential stiffness of aneurysms with respect to healthy arterial wall, and the axial displacement of the aortic root, the diameter may lower between diastole and systole, which explains why several patients have a negative DC_A (Figure 5). As pointed out by others, the axial dimension is an often-overlooked parameter.²⁶ It is not possible to relate the axial stretch to any kind of measurable axial load. Therefore, the volume-based distensibility DC_V was defined and relates the pressure increase, the only measurable information on the load exerted on the tissue, to the total volume change of the aneurysm. As can be seen in Figure 5 and Table 2, DC_V correlates even better with the failure risk DFR_i in both directions as compared with DC_A .

To enhance the reliability of our risk assessment, we introduced an alternative metric called probabilistic failure risk (PFR_i), which accounts for uncertainties in blood

TABLE 1. Baseline characteristics²¹

Variable	Population (n = 33)	$DC_A \leq DC_A^{phys}$ (n = 16)	$DC_A > DC_A^{phys}$ (n = 17)
General			
Age, y*	58.1 ± 19.8	68.8 ± 14.1	51.1 ± 14.9
Weight, kg	81.7 ± 24.9	80.4 ± 24.3	81.7 ± 23.1
Height, m*	1.74 ± 0.09	1.69 ± 0.09	1.76 ± 0.03
Sex: female	9 (27%)	7 (44%)	2 (12%)
Hypertension	21 (64%)	12 (75%)	9 (53%)
BAV	17 (52%)	9 (56%)	8 (47%)
TAV	16 (48%)	7 (44%)	9 (53%)
Aortic valve stenosis	14 (42%)	7 (44%)	7 (41%)
Aortic valve insufficiency	21 (64%)	10 (62%)	11 (65%)
Aortic regurgitation (II, III, IV)	18 (55%)	8 (50%)	10 (59%)
P_{dias} , mm Hg	72 ± 14	70.5 ± 15.2	73 ± 10
P_{sys} , mm Hg*	131 ± 32	145 ± 22.3	117 ± 19
Geometrical			
D_{dias} , mm*	47.5 ± 12.6	52.4 ± 11.4	45.3 ± 6.79
D_{sys} , mm*	48.1 ± 13	52.9 ± 11.6	47.5 ± 6.04
$\frac{D_{sys}}{D_{dias}}$, -*	1.03 ± 0.0442	1.01 ± 0.00732	1.05 ± 0.0352
L_{dias} , mm*	76 ± 21.5	85.6 ± 16.9	71.6 ± 16.5
L_{sys} , mm*	82.1 ± 17.2	86.2 ± 14.8	76 ± 17
$\frac{L_{sys}}{L_{dias}}$, -*	1.08 ± 0.08	1.04 ± 0.06	1.09 ± 0.05
V_{dias} , cm ³ *	107 ± 78.4	150 ± 51.9	98.2 ± 60.5
V_{sys} , cm ³ *	130 ± 82.5	160 ± 64.9	119 ± 55.7
$\frac{V_{sys}}{V_{dias}}$, -*	1.14 ± 0.16	1.1 ± 0.06	1.21 ± 0.12
$AHI \cdot 10^{-2}$, -*	2.84 ± 0.64	3.14 ± 0.90	2.69 ± 0.49
$ASI \cdot 10^{-5}$, mm ⁻¹ *	2.53 ± 0.84	2.93 ± 0.71	2.34 ± 0.46
Histologic			
Intimal hyperplasia	12 (36%)	8 (50%)	4 (24%)
Medial degeneration	9 (27%)	7 (44%)	2 (12%)
Total wall thickness, mm	1.71 ± 0.366	1.7 ± 0.399	1.73 ± 0.27
Intima thickness, mm*	0.06 ± 0.22	0.073 ± 0.46	0.040 ± 0.07
Media thickness, mm	1.24 ± 0.241	1.2 ± 0.36	1.29 ± 0.21
Adventitia thickness, mm	0.412 ± 0.15	0.44 ± 0.16	0.41 ± 0.13
Elastin, %	22.5 ± 18.2	20.5 ± 19.6	23.8 ± 16.5
Collagen, %	30.5 ± 12.8	32.3 ± 15.3	29.4 ± 9.14
Mechanical			
$Y_{\theta\theta}$, MPa*	1.510 ± 1.030	0.834 ± 0.795	1.900 ± 1.110
Y_{zz} , MPa	0.587 ± 0.232	0.567 ± 0.253	0.607 ± 0.184
$PWS_{\theta\theta}$, MPa	0.177 ± 0.090	0.186 ± 0.102	0.156 ± 0.057
PWS_{zz} , MPa	0.076 ± 0.110	0.121 ± 0.088	0.053 ± 0.033
$DC_A \cdot 10^{-3}$, mm Hg ⁻¹ *	1.43 ± 1.98	0.22 ± 0.30	2.20 ± 1.05
$DC_V \cdot 10^{-3}$, mm Hg ⁻¹ *	2.77 ± 2.88	1.25 ± 1.28	4.09 ± 3.26
DFR_{θ} , -*	0.138 ± 0.098	0.164 ± 0.196	0.073 ± 0.053
DFR_{zz} , -*	0.148 ± 0.204	0.275 ± 0.095	0.073 ± 0.021
PFR_{θ} , -*	-91.7 ± 60.8	-56.0 ± 54.2	-114.0 ± 39.8
PFR_{zz} , -*	-40.8 ± 73.7	-17.2 ± 8.7	-95.0 ± 39.6

Results are shown as median ± interquartile range or as number of patients (percentage). D_{dias} and D_{sys} and refer to the maximal aortic diameter measured at diastole and systole, respectively. Aortic regurgitation was classified according to the guidelines presented in Zoghbi and colleagues.²¹ BAV, Bicuspid aortic valve; TAV, tricuspid aortic valve; P_{dias} , diastolic pressure; P_{sys} , systolic pressure; -, dimensionless; L_{dias} , axial length of the aneurysm at diastole; L_{sys} , axial length of the aneurysm at systole; V_{dias} , aneurysm volume at diastole; V_{sys} , aneurysm volume at systole; AHI , aortic height index; ASI , aortic size index; PWS , peak wall stress; DC , distensibility coefficient; DFR , deterministic failure risk; PFR , probabilistic failure risk. * $P < .01$.

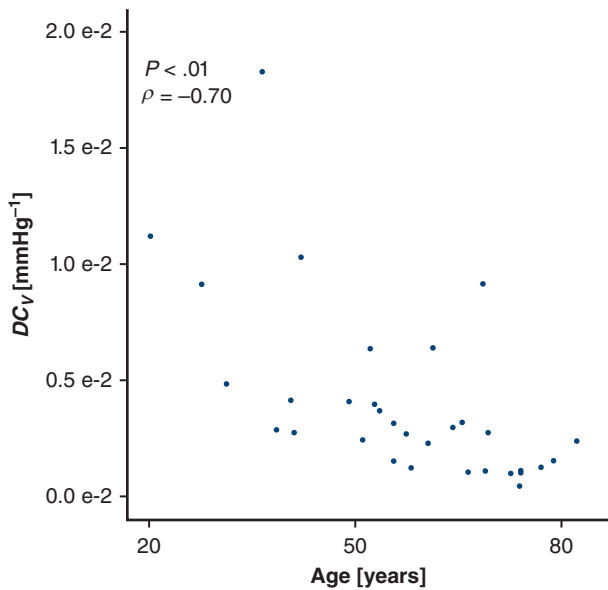


FIGURE 4. Volume-based distensibility (DC_V) in function of age.

pressure measurements and in vivo thickness estimation. The results from the probabilistic approach, presented in Appendix E4, align with the deterministic assessment and confirm our findings.

It is worth noting that “stiff” aneurysms exhibit significantly larger diameters compared with the “compliant” aorta (Table 1). However, as a positive correlation is not a transitive property, this does not imply that diameter alone is a reliable predictor for aneurysm wall failure.²⁷ This is further supported by our findings presented in Figure 5 and Table 2, which demonstrate that the correlation between diameter and failure risk is nonsignificant, in contrast to the significant correlation between distensibility and failure risk.

Implications for Surgical Guidelines

The presented results have important implications, suggesting the necessity of visualizing the aorta at both diastole and systole. Only by correlating the deformation between these 2 phases with the measured luminal pressures can the aortic distensibility be assessed in vivo.²⁸ Therefore, we recommend considering the incorporation of multiphasic scans into clinical practice when diagnosing patients

with aneurysm. In addition, clinical practice should not only focus on the circumferential changes of the aneurysm, ie, related to the diameter, but also on axial and volumetric changes. Moreover, the distensibility needs to be measured consistently and accurately. This requires the use of dedicated software to segment the aorta at the time points of interest. A 3-dimensional reconstruction of the aneurysm allows for an accurate measurement not only of its volume but also its diameter.²⁹ The blood pressures (typically at diastole and systole) must correspond to the appropriate phases at which the aneurysm is segmented and consistently measured.^{14,30}

According to Figure 4, the distensibility decreases with age, which is in accordance with Koullias and colleagues.¹⁶ Therefore, age seems to have an indirect effect on the failure risk due to the corresponding arterial remodeling and stiffening. Depending on their distensibility, older patients may be at greater risk for rupture or dissection and be more eligible for aortic repair. In this regard, it is important to note that Zierer and colleagues³¹ found that elective repair in patients of advanced age, ie, older than 70 years, does not impair functional recovery.

Limitations and Future Work

Despite the recommendations, it is important to acknowledge that validation studies are essential before implementing these practices in routine clinical care. Furthermore, in the presented study, it was assumed that blood flow patterns do not affect the acute failure risk. Indeed, although it has been found that elevated wall shear stresses can induce wall remodeling processes,³² we hypothesize that these are of lesser importance when assessing the risk of acute rupture or dissection. This same assumption allowed us to mix different etiologies in an attempt to identify common predictors. Still, further research is required to study the underlying mechanisms and pathophysiology of the ascending thoracic aortic aneurysm to further increase our understanding of how the disease progresses and differentiate risk stratification accordingly.

The R^2 values describing the simple logistic regression between the failure risk and the distensibility coefficients were low to moderate. In addition, multivariate logistic regression analysis found no significant combinations of predictors that help to predict the failure risk. Therefore,

TABLE 2. Spearman coefficients with corresponding P values of the correlation between the deterministic failure risk (DFR_i) and clinically accessible characteristics

	Age		D_{sys}		L_{sys}		V_{sys}		AHI		ASI		DC_A		DC_V	
	ρ	P	ρ	P	ρ	P	ρ	P	ρ	P	ρ	P	ρ	P	ρ	P
DFR_ρ	0.45	.06	0.44	.07	0.24	.33	0.52	.03	0.54	.02	0.45	.06	-0.56	.018	-0.59	.01
DFR_z	0.36	.26	0.29	.35	-0.26	.42	0.06	.85	0.31	.33	0.31	.33	-0.68	.019	-0.80	.003

Significant P values are shown in bold. D_{sys} , Maximal aortic diameter measured at systole; L_{sys} , axial length of the aneurysm at systole; V_{dias} , aneurysm volume at diastole; V_{sys} , aneurysm volume at systole; AHI, aortic height index; ASI, aortic size index; DC_A , area-based distensibility coefficient; DC_V , volume-based distensibility coefficient.

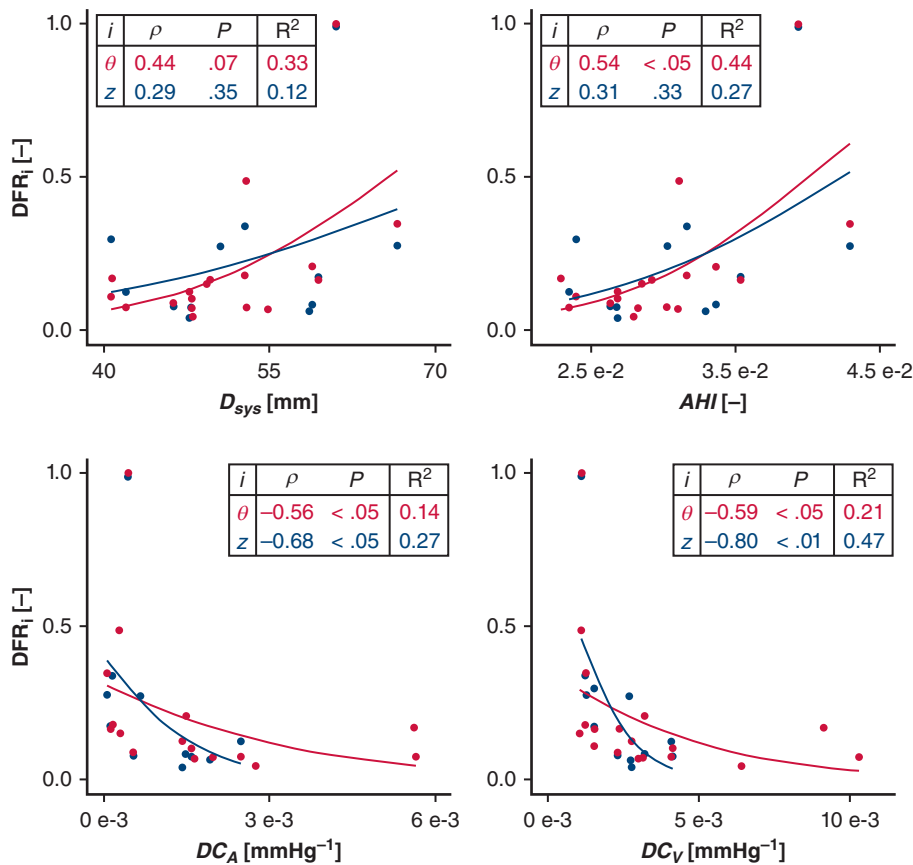


FIGURE 5. Deterministic failure risk DFR_i in the circumferential (red) and axial direction (blue) with respect to D_{sys} (top left), AHI (top right), DC_A (bottom left), and DC_V (bottom right). For each of the predictors in both directions, the Spearman correlation coefficient with corresponding P value is given, together with the Nagelkerke pseudo R^2 value of the logistic regression. D_{sys} , Maximal aortic diameter measured at systole; AHI , aortic height index; DC_A , area-based distensibility coefficient; DC_V , volume-based distensibility coefficient.

it is not yet possible to determine with sufficient confidence the critical range of predictor values that distinguish stable aneurysms from aneurysms that are likely to rupture or dissect, or even aneurysms from healthy aortas.³³ To do so, more patients are required in the clinical study. The limited data set may also explain why no significant correlations were found between the distensibility coefficient and other cardiovascular characteristics such as aortic valve stenosis, insufficiency and regurgitation (Table 1).

We have chosen for uniaxial tensile testing to estimate the strength of the tissue. Whereas other measurement techniques exist,⁹ uniaxial tensile testing is a widely accepted method to estimate the strength of the tissue.³⁴ The benefit of hourglass-shaped samples is that tear will more likely occur at the center of the sample instead of the regions near the clamps due to stress concentrations caused by the test design. The downside of this shape is that deformation at the gauge region is highly inhomogeneous. Consequently, we were only able to express the failure risk in terms of the (nominal) stress but not in terms of the

deformation. It is important to note that the stress measured at yield did not always align with the maximal stress observed during the test. In certain samples, the yield point coincided with partial tearing of some of the medial layers, ie, dissection. Consequently, stress levels greater than this yield point might have been recorded. In contrast, other samples experienced an immediate tear throughout the entire wall, ie, rupture. This discrepancy in outcomes (rupture or dissection) is why the term “wall failure” was used.

Although we measured the ex vivo thickness and mechanical behavior of different tissue sample along the aneurysm circumference, we fitted a single material model to the experimental results. Moreover, we could excise only up to 2 samples for uniaxial testing (one for each principal direction), and thus did not explicitly account for tissue heterogeneity.³⁵ We modeled the aneurysms as an axisymmetric homogeneous thin-walled cylinder. The influence of other irregular geometric features such as arterial tortuosity³⁶ and spatial-dependent material characteristics can be

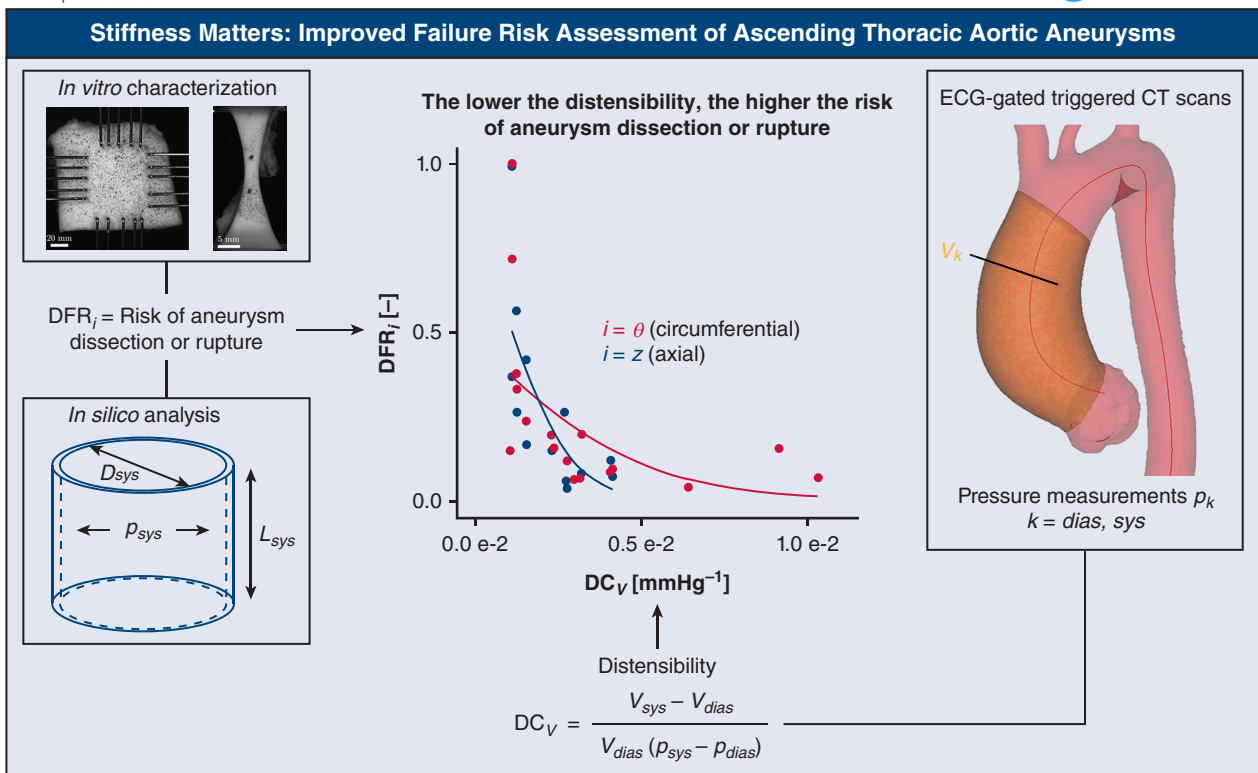


FIGURE 6. A combined in vivo, in silico and in vitro approach revealed that the volumetric distensibility correlates strongly with the aneurysm failure risk. ECG, Electrocardiogram; CT, computed tomography;

modeled using finite element modelling, but did not fall within the scope of the presented study.

CONCLUSIONS

By conducting a retrospective personalized failure risk assessment of patients with ATAA, we were able to identify and compare clinically accessible aneurysm failure risk predictors. Mechanical predictors, ie, the distensibility coefficients, outperform predictors based on geometrical features alone in predicting wall failure (Figure 6). The volume-based DC has the best predictive power, as it also takes the axial stretch into account. This study provides supporting evidence to include multiphasic scans in clinical practice for assessing the risk of aneurysm failure. Clinicians can implement this new metric in their risk-stratification process, where it can gradually replace purely geometrical predictors as the database and hence confidence in a cut-off value grows.

Data Availability Statement

The data set presented in this study is publicly available in KU Leuven RDR. The data can be found here: <https://doi.org/10.48804/41RAQA>.

Use of Artificial Intelligence in the Writing Process

During the preparation of this work, the authors used ChatGPT-3.5 in order to enhance clarity. After using this tool/service, the authors reviewed and edited the content as needed and take full responsibility for the content of the publication.

Conflict of Interest Statement

The authors reported no conflicts of interest. The *Journal* policy requires editors and reviewers to disclose conflicts of interest and to decline handling or reviewing manuscripts for which they may have a conflict of interest. The editors and reviewers of this article have no conflicts of interest.

The authors thank Liselotte Peeters for her help in performing and processing the mechanical experiments, Kimberly Crevits for her help in performing the mechanical experiments, and Ruben Snoeck for his help in performing the histological analysis and the segmentation of the computed tomography scans.

References

1. Isselbacher EM. Thoracic and abdominal aortic aneurysms. *Circulation*. 2005; 111:816-28.

2. Isselbacher EM, Preventza O, Black JH, Augoustides JG, Beck AW, Bolen MA, et al. 2022 ACC/AHA Guideline for the diagnosis and management of aortic disease: a report of the American Heart Association/American College of Cardiology joint committee on clinical practice guidelines. *Circulation*. 2022;146:e334-482.
3. Sherifova S, Holzapfel GA. Biomechanics of aortic wall failure with a focus on dissection and aneurysm: a review. *Acta Biomater*. 2019;99:1-17. <https://doi.org/10.1016/j.actbio.2019.08.017>
4. Pape LA, Tsai TT, Isselbacher EM, Oh JK, O'Gara PT, Evangelista A, et al. Aortic diameter >5.5 cm is not a good predictor of type A aortic dissection. *Circulation*. 2007;116:1120-7. <https://doi.org/10.1161/CIRCULATIONAHA.107.702720>
5. Kontopodis N, Pantidis D, Dedes A, Daskalakis N, Ioannou CV. The—not so—solid 5.5 cm threshold for abdominal aortic aneurysm repair: facts, misinterpretations, and future directions. *Front Surg*. 2016;3:1.
6. Davies RR, Gallo A, Coady MA, Tellides G, Botta DM, Burke B, et al. Novel measurement of relative aortic size predicts rupture of thoracic aortic aneurysms. *Ann Thorac Surg*. 2006;81:169-77.
7. Zafar MA, Li Y, Rizzo JA, Charilaou P, Saeyeldin A, Velasquez CA, et al. Height alone, rather than body surface area, suffices for risk estimation in ascending aortic aneurysm. *J Thorac Cardiovasc Surg*. 2018;155:1938-50. <https://doi.org/10.1016/j.jtcvs.2017.10.140>
8. Wu J, Zafar MA, Li Y, Saeyeldin A, Huang Y, Zhao R, et al. Ascending aortic length and risk of aortic adverse events: the neglected dimension. *J Am Coll Cardiol*. 2019;74:1883-94.
9. Duprey A, Trabelsi O, Vola M, Favre JP, Avril S. Biaxial rupture properties of ascending thoracic aortic aneurysms. *Acta Biomater*. 2016;42:273-85.
10. Martin C, Sun W, Pham T, Elefteriades J. Predictive biomechanical analysis of ascending aortic aneurysm rupture potential. *Acta Biomater*. 2013;9:9392-400.
11. Tyrrell DJ, Chen J, Li BY, Wood SC, Rosebury-Smith W, Remmer HA, et al. Aging alters the aortic proteome in health and thoracic aortic aneurysm. *Arterioscler Thromb Vasc Biol*. 2022;42:1060-76.
12. Elefteriades JA, Rizzo JA, Zafar MA, Ziganshin BA. Ascending aneurysmectomy: should we shift to the left? *J Thorac Cardiovasc Surg*. 2023;166:435-41. <https://doi.org/10.1016/j.jtcvs.2022.07.033>
13. Halushka MK, Angelini A, Bartoloni G, Basso C, Batoroeva L, Bruneval P, et al. Consensus statement on surgical pathology of the aorta from the Society for Cardiovascular Pathology and the Association for European Cardiovascular Pathology: II. Noninflammatory degenerative diseases - nomenclature and diagnostic criteria. *Cardiovasc Pathol*. 2016;25:247-57.
14. Bons LR, Duijnhouwer AL, Boccacini S, van den Hoven AT, van der Vlugt MJ, Chelu RG, et al. Intermodality variation of aortic dimensions: how, where and when to measure the ascending aorta. *Int J Cardiol*. 2019;276:230-5. <https://doi.org/10.1016/j.ijcard.2018.08.067>
15. Mosteller R. Simplified calculation of body-surface area. *N Engl J Med*. 1987;317:1098. <https://doi.org/10.1056/NEJM198710223171717>
16. Koullias G, Modak R, Tranquilli M, Korkolis DP, Barash P, Elefteriades JA. Mechanical deterioration underlies malignant behavior of aneurysmal human ascending aorta. *J Thorac Cardiovasc Surg*. 2005;130:677.e1-9.
17. Vander Linden K, Fehervary H, Vastmans J, Famaey N. The influence of out-of-plane motion on the deformation measurement of planar biaxial tests on biological soft tissue. *Mech Res Commun*. 2023;129:104099. <https://doi.org/10.1016/j.mechrescom.2023.104099>
18. Maes L, Fehervary H, Vastmans J, Mousavi SJ, Avril S, Famaey N. Constrained mixture modeling affects material parameter identification from planar biaxial tests. *J Mech Behav Biomed Mater*. 2019;95:124-35.
19. Vander Linden K, Fehervary H, Maes L, Famaey N. An improved parameter fitting approach of a planar biaxial test including the experimental prestretch. *J Mech Behav Biomed Mater*. 2022;134:105389.
20. Polzer S, Gasser TC. Biomechanical rupture risk assessment of abdominal aortic aneurysms based on a novel probabilistic rupture risk index. *J Roy Soc Interface*. 2015;12:20150852.
21. Zoghbi WA, Adams D, Bonow RO, Enriquez-Sarano M, Foster E, Grayburn PA, et al. Recommendations for noninvasive evaluation of native valvular regurgitation: a report from the American Society of Echocardiography developed in collaboration with the Society for Cardiovascular Magnetic Resonance. *J Am Soc Echocardiogr*. 2017;30:303-71. <https://doi.org/10.1016/j.echo.2017.01.007>
22. Bai W, Suzuki H, Huang J, Francis C, Wang S, Tarroni G, et al. A population-based phenome-wide association study of cardiac and aortic structure and function. *Nat Med*. 2020;26:1654-62.
23. Goldfinger JZ, Halperin JL, Marin ML, Stewart AS, Eagle KA, Fuster V. Thoracic aortic aneurysm and dissection. *J Am Coll Cardiol*. 2014;64:1725-39.
24. Emerel L, Thunes J, Kickliter T, Billaud M, Phillippi JA, Vorp DA, et al. Predissection-derived geometric and distensibility indices reveal increased peak longitudinal stress and stiffness in patients sustaining acute type A aortic dissection: implications for predicting dissection. *J Thorac Cardiovasc Surg*. 2019;158:355-63.
25. Fortunato RN, Huckaby LV, Emerel LV, Schlosser V, Yang F, Phillippi JA, et al. The predictive capability of aortic stiffness index for aortic dissection among dilated ascending aortas. *J Thorac Cardiovasc Surg*. September 12, 2022. [Epub ahead of print]. <https://doi.org/10.1016/j.jtcvs.2022.09.003>
26. Guala A, Teixidó-Tura G, Rodríguez-Palomares J, Ruiz-Muñoz A, Dux-Santoy L, Villalva N, et al. Proximal aorta longitudinal strain predicts aortic root dilation rate and aortic events in Marfan syndrome. *Eur Heart J*. 2019;40:2047-55.
27. Langford E, Schwertman N, Owens M. Is the property of being positively correlated transitive? *Am Stat*. 2001;55:322-5. <https://doi.org/10.1198/000313001753272286>
28. Brunner-La Rocca HP. Towards applicability of measures of arterial stiffness in clinical routine. *Eur Heart J*. 2010;31:2320-2.
29. Manning BJ, Kristmundsson T, Sonesson B, Resch T. Abdominal aortic aneurysm diameter: a comparison of ultrasound measurements with those from standard and three-dimensional computed tomography reconstruction. *J Vasc Surg*. 2009;50:263-8.
30. Elefteriades JA, Mukherjee SK, Mojibian H. Discrepancies in measurement of the thoracic aorta: JACC review topic of the week. *J Am Coll Cardiol*. 2020;76:201-17.
31. Zierer A, Melby SJ, Lubahn JG, Sicard GA, Damiano RJ, Moon MR. Elective surgery for thoracic aortic aneurysms: late functional status and quality of life. *Ann Thorac Surg*. 2006;82:573-8.
32. Salmasi MY, Pirola S, Sasidharan S, Fisichella SM, Redaelli A, Jarral OA, et al. High wall shear stress can predict wall degradation in ascending aortic aneurysms: an integrated biomechanics study. *Front Bioeng Biotechnol*. 2021;9:1-13.
33. Mattace-Raso FUS, Hofman A, Verwoert GC, Wittemana JCM, Wilkinson I, Cockcroft J, et al. Determinants of pulse wave velocity in healthy people and in the presence of cardiovascular risk factors: 'establishing normal and reference values'. *Eur Heart J*. 2010;31:2338-50.
34. Macrae RA, Miller K, Doyle BJ. Methods in mechanical testing of arterial tissue: a review. *Strain*. 2016;52:380-99.
35. Lin S, Morgant MC, Marín-Castrillón DM, Walker PM, Aho Glélé LS, Boucher A, et al. Aortic local biomechanical properties in ascending aortic aneurysms. *Acta Biomater*. 2022;149:40-50.
36. Alhafez BA, Truong VTT, Ocazionez D, Sohrabi S, Sandhu H, Estrera A, et al. Aortic arch tortuosity, a novel biomarker for thoracic aortic disease, is increased in adults with bicuspid aortic valve. *Int J Cardiol*. 2019;284:84-9. <https://doi.org/10.1016/j.ijcard.2018.10.052>

Key Words: ascending thoracic aortic aneurysm, risk assessment, surgical guidelines, aortic compliance, rupture, dissection

APPENDIX E1. EXPERIMENTAL PROTOCOLS OF THE UNIAXIAL AND PLANAR BIAxIAL TENSILE TEST

Uniaxial Tensile Test

Hourglass samples were mounted on a uniaxial test set-up using clamps. The clamp-to-clamp separation at the start of the uniaxial test was 30 mm. The protocol consisted of multiple displacement-controlled loading steps: 5%, 10%, 15%, 20%, 25%, 50% nominal strain and until rupture, applied at a linear rate of 5%/s. Every loading step consisted of 5 loading cycles to precondition the tissue. A preload of 0.05 N was applied to flatten the sample. Two markers were applied at the gauge region to track the deformation.

Planar Biaxial Tensile Test

Square samples were mounted on a planar biaxial testing set-up using rakes. The rakes consisted of 4 sets of 5 parallel needles, each rake spaced 1 mm apart. The sample's circumferential and axial axes were aligned with the horizontal and vertical testing axes, respectively. The rake-to-rake separation at the start of the test was 7 mm. A displacement-controlled loading protocol was used consisting of 6 loading steps: 5%, 10%, 15%, 20%, 25%, and 35% nominal strain, applied at a linear rate of 5%/s. Each loading step was repeated three times, while changing the relative applied loading between the circumferential and axial direction: 1:1; 2:1, and 1:2. Each loading step consisted of four preconditioning cycles and one loading cycle used for further analysis. Before every loading cycle, a preload of 0.05 N was applied in both directions to avoid buckling. Using graphite powder, a speckle pattern was applied to the biaxial samples to track the deformation using digital image correlation (DIC). Incremental DIC was performed using VIC-2D (Correlated Solutions) with a subset of 97 pixels and a step size of 7 pixels. The deformation gradient throughout the experiment was calculated based on the DIC results of the central 25% of the area enclosed by the rakes, assuming homogeneous deformation.^{E1} Experimental forces in the circumferential ($f_{\theta\theta}$) and longitudinal direction (f_{zz}) were captured at 20 Hz and calculated as the average force measured by the horizontally and vertically opposed actuators, respectively. For every ratio, the fifth loading cycle of the last loading step was processed.

APPENDIX E2. MECHANICAL ANALYSIS

Material Description

The Cauchy model stress σ^{mod} is calculated as follows:

$$\sigma^{mod} = \frac{\partial \Psi}{\partial \mathbf{F}} \mathbf{F}^T - b \mathbf{I}. \quad (4)$$

In this equation, Ψ represents the strain energy of the described material, \mathbf{F} the total deformation with respect to

a reference state, \mathbf{I} the identity matrix and b a Lagrange multiplier. The stresses (both in vivo and in vitro) are calculated using the plane stress assumption, ie, the stress in the radial direction r equals zero: $\sigma_{rr}^{mod} = 0$, which determines the value of b .

The Gasser–Ogden–Holzapfel^{E2} constitutive material model in the context of the constrained mixture theory is used to calculate the strain energy. The aneurysmal tissue is modelled as a mixture consisting of two constituents: the noncollagenous isotropic matrix (e) and collagen fibres (c). The strain energy function is described as:

$$\Psi = C_{10} \left(I_1^{(e)} - 3 \right) + \frac{k_1}{2k_2} \sum_{i=4,6} \left[\exp \left(k_2 \left[\left(\kappa I_1^{(c)} + (1-3\kappa) I_i^{(c)} \right) - 1 \right]^2 \right) - 1 \right] \quad (5)$$

with:

$$I_1^{(j)} = \text{tr}(\mathbf{C}^{(j)}), j = e, c,$$

$$I_i^{(c)} = \mathbf{C}^{(c)} : \mathbf{M}_i \otimes \mathbf{M}_i, i = 4, 6,$$

$$\mathbf{M}_4 = [0, \cos \alpha, \sin \alpha]^T; \mathbf{M}_6 = [0, \cos \alpha, -\sin \alpha]^T,$$

$$\mathbf{C}^{(j)} = \mathbf{F}^{(j)T} \mathbf{F}^{(j)}, \quad (6)$$

and with $\mathbf{F}^{(j)} = \mathbf{F} \mathbf{G}^{(j)}$ representing the elastic deformation experienced by constituent $j=e,c$ which consists of the total deformation of the mixture w.r.t. the diastolic reference configuration (\mathbf{F}) and the constituent specific deposition stretch tensor ($\mathbf{G}^{(j)}$). Figure E1 shows an overview of the different loading states. The parameter set s contains the 5 material properties, $C_{10}, k_1, k_2, \kappa, \alpha$, representing the matrix stiffness, fiber stiffness, fiber stiffening, fiber dispersion, and fiber angle w.r.t. circumferential direction, respectively. The deposition stretch of collagen $\mathbf{G}^{(c)}$ is assumed to be known^{E3}:

$$\mathbf{G}_i^{(c)} = g^{(c)} \mathbf{M}_i \otimes \mathbf{M}_i + \frac{1}{\sqrt{g^{(c)}}} (\mathbf{I} - \mathbf{M}_i \otimes \mathbf{M}_i), i = 4, 6, g^{(c)} = 1.1 \quad (7)$$

Assuming isochoric deformation:

$$\mathbf{G}^{(e)} = \begin{bmatrix} \frac{1}{g_{\theta\theta}^{(e)} g_{zz}^{(e)}} & 0 & 0 \\ 0 & g_{\theta\theta}^{(e)} & 0 \\ 0 & 0 & g_{zz}^{(e)} \end{bmatrix}. \quad (8)$$

In the current study, the axial deposition stretch $g_{zz}^{(e)}$ is derived from literature, as function of the patient's age,^{E4} whereas the circumferential deposition stretch $g_{\theta\theta}^{(e)}$ is calculated based on the condition of static equilibrium of the geometry experiencing the internal pressure at diastole p_{dias} .^{E5} For a given s , H_{dias} , p_{dias} and $\mathbf{F}=\mathbf{I}$, and using the nonlinear equation solver 'fsolve' in MATLAB R2023a, $g_{\theta\theta}^{(e)}$ can be solved from the following:

$$p_{dias} = \frac{2\sigma_{\theta\theta}^{mod} H_{dias}}{D_{dias}}. \quad (9)$$

Parameter Fitting

The material parameters s and diastolic thickness H_{dias} are found by minimizing the objective O in the following equation:

$$O = \frac{w_1}{3nN} \sum_{s=1}^N \sum_{r=1}^3 \sum_{j=1}^n \left[\left(\frac{f_{\theta\theta}^{mod}(t_{j,r}) - \overline{f_{\theta\theta}}(t_{j,r})}{\overline{f_{\theta\theta}}} \right)^2 + \left(\frac{f_{zz}^{mod}(t_{j,r}) - \overline{f_{zz}}(t_{j,r})}{\overline{f_{zz}}} \right)^2 \right]_s + \frac{w_2}{N} \sum_{s=1}^N \left[\left(\frac{H_0^{mod} - H_0}{H_0} \right)^2 \right]_s + w_3 \left(\frac{p_{sys}^{mod} - p_{sys}}{p_{sys}} \right)^2, \quad (10)$$

with $f_{ii}^{mod}(t_{j,r})$ and $f_{ii}(t_{j,r})$ the model and experimental forces in the direction $i=\theta,z$ during the planar biaxial experiment at time point $t_{j,r}$. j determines the index of the loading cycle at ratio r , n the total number of time points of a loading cycle, s the sample index, and N the total number of samples excised from the aneurysm. The weights w_1, w_2 , and w_3 were set to 0.4, 0.3, and 0.3, respectively. $\overline{f_{ii}}$ ($i=\theta,z$) indicates the mean of all experimental forces along the i th direction. f_{ii}^{mod} is calculated as follows:

$$f_{ii}^{mod} = P_{0,ii}^{mod} a_{0,i}, \quad (11)$$

with $a_{0,i}$ the cross-sectional area in the zero-stress state with its normal along i th direction. $P_{0,ii}^{mod}$ is the first Piola-Kirchhoff stress along i th direction pulled back to the zero-stress state and is calculated according to:

$$\mathbf{P}_0^{mod} = \boldsymbol{\sigma}^{mod} (\mathbf{F}\mathbf{F}_{rel}^{-1})^{-T}, \quad (12)$$

with $\mathbf{F}=\mathbf{F}_{biax}\mathbf{F}_{rel}$, where \mathbf{F}_{biax} is the deformation between the zero-stress state and the biaxially loaded state, and \mathbf{F}_{rel} the deformation between the reference and the zero-stress state, see Figure E1.

To calculate f_{ii}^{mod} , one should identify \mathbf{F}_{rel} and \mathbf{F}_{biax} . Once the diastolic reference configuration is prestressed using $\mathbf{G}^{(c)}$ and $\mathbf{G}^{(e)}$, \mathbf{F}_{rel} , defined as

$$\mathbf{F}_{rel} = \begin{bmatrix} \lambda_{rel,rr} & 0 & 0 \\ 0 & \lambda_{rel,\theta\theta} & 0 \\ 0 & 0 & \lambda_{rel,zz} \end{bmatrix} \quad (13)$$

can be derived from the condition that $\sigma_{ii}^{mod} = 0$ ($i=\theta,z$). Assuming isochoric deformation, ie, $\lambda_{rel,rr} = \frac{1}{\lambda_{rel,\theta\theta}\lambda_{rel,zz}}$, $\lambda_{rel,\theta\theta}$, and $\lambda_{rel,zz}$ are calculated using the nonlinear equation solver 'fsolve' in Matlab R2023a. Knowing \mathbf{F}_{rel} , the model thickness in the zero-stress state is then calculated as $H_0^{mod} = H_{dias}\lambda_{rel,rr}$

$\mathbf{F}_{biax}=\mathbf{F}_{LC}\mathbf{F}_p$, where \mathbf{F}_p is the deformation caused by the preloading of the sample before the loading cycle, see Vander Linden and colleagues.¹⁹ No shear deformation during biaxial testing is assumed:

$$\mathbf{F}_{LC} = \begin{bmatrix} \frac{1}{\lambda_{LC,\theta\theta}\lambda_{LC,zz}} & 0 & 0 \\ 0 & \lambda_{LC,\theta\theta} & 0 \\ 0 & 0 & \lambda_{LC,zz} \end{bmatrix}, \quad (14)$$

$$\mathbf{F}_p = \begin{bmatrix} \frac{1}{\lambda_{p,\theta\theta}\lambda_{p,zz}} & 0 & 0 \\ 0 & \lambda_{p,\theta\theta} & 0 \\ 0 & 0 & \lambda_{p,zz} \end{bmatrix}.$$

$\lambda_{LC,\theta\theta}$ and $\lambda_{LC,zz}$ are experimentally measured by performing DIC between a biaxially loaded state and the preloaded state. $\lambda_{p,\theta\theta}$ and $\lambda_{p,zz}$ are derived from the condition that $f_{ii}^{mod} = f_{ii}(t_1, r)$ ($i = \theta, z$) at each ratio r , using the nonlinear equation solver 'fsolve' in Matlab R2023a.¹⁹

$a_{0,i}$ used in the equation to calculate the model force, is determined as:

$$a_{0,r} = \frac{l_{p,z}l_{p,\theta}}{\lambda_{p,zz}\lambda_{p,\theta\theta}},$$

$$a_{0,\theta} = \frac{H_0 l_{p,z}}{\lambda_{p,zz}},$$

$$a_{0,z} = \frac{H_0 l_{p,\theta}}{\lambda_{p,\theta\theta}}, \quad (15)$$

with $l_{p,z}$ and $l_{p,\theta}$ the rake-to-rake distance in the preloaded state in the axial and circumferential direction, respectively.

The Cauchy stress at systole σ_{sys}^{mod} is calculated for a given s , $\mathbf{G}^{(c)}$, $\mathbf{G}^{(e)}$ and $\mathbf{F}=\mathbf{F}_{sys}$, with

$$\mathbf{F}_{sys} = \begin{bmatrix} 1 & 0 & 0 \\ \frac{1}{\lambda_{sys,\theta\theta}^{avg} \lambda_{sys,zz}} & 0 & 0 \\ 0 & \lambda_{sys,\theta\theta}^{avg} & 0 \\ 0 & 0 & \lambda_{sys,zz} \end{bmatrix}, \quad (16)$$

where $\lambda_{sys,zz} = \frac{L_{sys}}{L_{dias}}$ represents the axial stretch between diastole and systole. Assuming an incompressible extension-inflation between diastole and systole^{E5}:

$$\lambda_{sys,\theta\theta}^{avg} = \frac{\sqrt{D_{sys}^2 + \frac{(D_{dias}+H_{dias})^2 - D_{dias}^2}{\lambda_{sys,zz}}}}{D_{dias}+H_{dias}}. \quad (17)$$

The model intraluminal systolic pressure is then: $p_{sys}^{mod} = \frac{2\sigma_{sys,\theta\theta}^{mod} H_{sys}}{D_{sys}}$, with $H_{sys} = \frac{H_{dias}}{\lambda_{sys,\theta\theta}^{avg} \lambda_{sys,zz}}$.

The objective O was minimized using the nonlinear least square solver in Matlab R2023a. 20 different start points are used to find a global minimum. The imposed boundaries on the parameters of s and H_{dias} are shown in Table E1. Because of the different ranges of the boundaries, the parameters were first scaled when performing the fitting. The fitting quality measures are defined through the use of the normalized root mean squared error (NRMSE):

$$NRMSE_{PB} = \frac{1}{f^{avg}} \sqrt{\frac{\sum_{s=1}^N \sum_{r=1}^3 \sum_{j=1}^n \left[(f_{\theta\theta}^{mod}(t_{j,r}) - f_{\theta\theta}(t_{j,r}))^2 + (f_{zz}^{mod}(t_{j,r}) - f_{zz}(t_{j,r}))^2 \right]_s}{3nN}},$$

$$NRMSE_{H_0} = \frac{1}{H_0^{avg}} \sqrt{\frac{\sum_{s=1}^N \left[(H_0^{mod} - H_0)^2 \right]_s}{N}},$$

$$NRMSE_{p_{sys}} = \left| \frac{p_{sys}^{mod} - p_{sys}}{p_{sys}} \right|, \quad (18)$$

with f^{avg} and H_0^{avg} the mean of all the measured forces and ex vivo thicknesses, respectively.

Calculating the Peak Wall Stresses and Failure Risks

Peak wall stresses and failure risks can be determined once the material parameters and in vivo thickness are fitted. Two main approaches are used for these calculations: a deterministic and a probabilistic approach.

Deterministic approach. In the deterministic approach, the calculation of peak wall stress assumes that no uncertainty affects the results. The aneurysm at diastole, pre-stressing it through $\mathbf{G}^{(c)}$ and $\mathbf{G}^{(e)}$, was assigned a thickness H_{dias} and material properties s . The aneurysm was further pressurized and axially stretched using $110\%p_{sys}$ and $\lambda_{def,zz} = \lambda_{sys,zz} = \frac{L_{sys}}{L_{dias}}$, respectively. This deformed state is characterized by the deformation gradient \mathbf{F}_{def} :

$$\mathbf{F}_{def} = \begin{bmatrix} 1 & 0 & 0 \\ \frac{1}{\lambda_{def,\theta\theta}^{avg} \lambda_{def,zz}} & 0 & 0 \\ 0 & \lambda_{def,\theta\theta}^{avg} & 0 \\ 0 & 0 & \lambda_{def,zz} \end{bmatrix},$$

$$\lambda_{def,\theta\theta}^{avg} = \frac{\sqrt{D_{def}^2 + \frac{(D_{dias}+H_{dias})^2 - D_{dias}^2}{\lambda_{def,zz}}}}{D_{dias}+H_{dias}}. \quad (19)$$

Using ‘fsolve’ in Matlab R2023a, the diameter in the deformed state D_{def} is calculated from the equation

$$1.10p_{sys} = \frac{2\sigma_{def,\theta\theta}^{mod} H_{def}}{D_{def}}, \quad \text{with } H_{def} = \frac{H_{dias}}{\lambda_{def,\theta\theta}^{avg} \lambda_{def,zz}}$$

thickness in the deformed state and $\sigma_{def,\theta\theta}^{mod}$ the circumferential component of σ_{def}^{mod} . σ_{def}^{mod} is solved from Eq. 4, using $s, \mathbf{G}^{(c)}, \mathbf{G}^{(e)}$ and $\mathbf{F}=\mathbf{F}_{def}$. The peak wall stress PWS_{ii} in the direction $i=\theta, z$ is defined as the i th component of \mathbf{P}_0^{mod} , according to Eq. 12 with $\mathbf{F}=\mathbf{F}_{def}$.

The resulting deterministic failure risk DFR_i in the direction $i=\theta, z$ is defined as the ratio between the peak wall stress PWS_{ii} and wall strength Y_{ii} , ie, $DFR_i = \frac{PWS_{ii}}{Y_{ii}}$.^{E6}

Probabilistic approach. The parameters used to calculate the peak wall stresses are subject to uncertainty which can arise from various sources, including inpatient variability or measurement uncertainty. To address this uncertainty, these parameters can be treated as stochastic variables. More specifically, the blood pressure is not measured at the same time at which the diameter is measured. To account for this, the diastolic blood pressure p_{dias} is assumed to follow a normal distribution (ρ_N):

$$\rho_{p_{dias}} \sim \rho_N(x) = \rho_N(\mu_x, SD_x^2) = \frac{1}{SD_x \sqrt{2\pi}} \exp\left(-\frac{1}{2} \left[\frac{x-\mu_x}{SD_x}\right]^2\right), \tag{20}$$

with $\mu_x = p_{dias}^{meas}$ the measured diastolic pressure (denoted with superscript ‘meas’) and $SD_x = SD_{p_{dias}} = 0.15 p_{dias}^{meas}$ the standard deviation representing the 24-hour blood pressure variability.^{E7} The pulse pressure is assumed to be constant throughout the day, ie, $p_{sys} = p_{dias} + (p_{sys}^{meas} - p_{dias}^{meas})$.

The in vivo wall thickness H_{dias} is fitted based on experimental data which are subject to measurement uncertainty. To account for this, H_{dias} is assumed to follow a lognormal distribution (ρ_{LN}):

$$\rho_{H_{dias}} \sim \rho_{LN}(x) = \rho_{LN}(\mu_x, SD_x^2) = \frac{1}{x SD_x \sqrt{2\pi}} \exp\left(-\frac{(\log x - \mu_x)^2}{2SD_x^2}\right), \tag{21}$$

with $\mu_x = \log(H_{dias}^{fit})$, $SD_x=0.29$ according to ^{E7} and H_{dias}^{fit} the diastolic wall thickness resulting from the parameter fitting procedure.

Using the Latin Hypercube Sampling method in the Sensitivity Analysis Library (SALib) in Python, the input space was discretized in 10,000 sampling points. Assuming a deterministic set of material properties s , the peak wall stresses were calculated for each sampling point, as explained in the previous section.

Based on the resulting PWS_{ii} data, a lognormal distribution $\rho_{PWS_{ii}}$ was fitted and its quality was verified using the Chi-Square Goodness-of-Fit Test. The resulting probabilistic failure risk PFR_i in the direction $i=\theta, z$ was calculated as follows^{E7}:

$$PFR_i = \log\left(\int_{Y_{ii}}^{+\infty} \rho_{PWS_{ii}}(x) dx\right) \tag{22}$$

assuming a deterministic wall strength Y_{ii} . The integral in Eq. 22 was numerically solved using the trapezoidal rule between 0 and 4 MPa with an interval of 1 kPa and represents the probability that the aneurysm ruptures or dissects in a single heartbeat. PFR_i values are negative, and as they approach zero, the likelihood of aneurysm failure increases, with zero representing a 100% chance. Figure E2 shows the results of the probabilistic approach for patient ATAA005.

APPENDIX E3. FITTED MATERIAL PARAMETERS

Table E2 shows an overview of the fitted parameters, fitted in vivo diastolic thickness and fitting quality measures $RMSE_{PB}, RMSE_{H_0}, RMSE_{p_{sys}}$. No PB test was performed for ATAA 6, 13 and 14.

APPENDIX E4. RESULTS OF THE PROBABILISTIC FAILURE RISK ASSESSMENT

Table E3 presents the Spearman ρ correlation coefficients with corresponding P values between the different clinically accessible characteristics and the failure risk PFR_i ($i=\theta, z$). Figure E3 shows the failure risk PFR_i ($i=\theta, z$) as function of D_{sys}, AHI, DC_A and DC_V . Spearman ρ correlation coefficient with corresponding P value and R^2 value of the linear regression is also shown in the Figure.

References

- E1. Fehervary H, Smoljkić M, Vander Sloten J, Famaey N. Planar biaxial testing of soft biological tissue using rakes: a critical analysis of protocol and fitting process. *J Mech Behav Biomed Mater.* 2016;61:135-51.
- E2. Gasser TC, Ogden RW, Holzapfel G. Hyperelastic modelling of arterial layers with distributed collagen fibre orientations. *J R Soc Interface.* 2006;3: 15-35.
- E3. Cyron CJ, Aydin RC, Humphrey JD. A homogenized constrained mixture (and mechanical analog) model for growth and remodeling of soft tissue. *Biomech Modeling Mechanobiol.* 2016;15:1389-403.
- E4. Horný L, Netušil M, Voňavková T. Axial prestretch and circumferential distensibility in biomechanics of abdominal aorta. *Biomech Modeling Mechanobiol.* 2014;13:783-99.
- E5. Vander Linden K, Ghasemi M, Maes L, Vastmans J, Famaey N. Layer-specific fiber distribution in arterial tissue modeled as a constrained mixture. *Int J Numer Method Biomed Eng.* 2022;39:e3608.
- E6. Smoljkić M, Fehervary H, Van den Bergh P, Jorge-Peñas A, Kluyskens L, Dymarkowski S, et al. Biomechanical characterization of ascending aortic aneurysms. *Biomech Modeling Mechanobiol.* 2017;16:705-20.
- E7. Polzer S, Kracik J, Novotný T, Kubíček L, Staffa R, Raghavan ML. Methodology for estimation of annual risk of rupture for abdominal aortic aneurysm. *Comput Methods Programs Biomed.* 2021;200:105916.

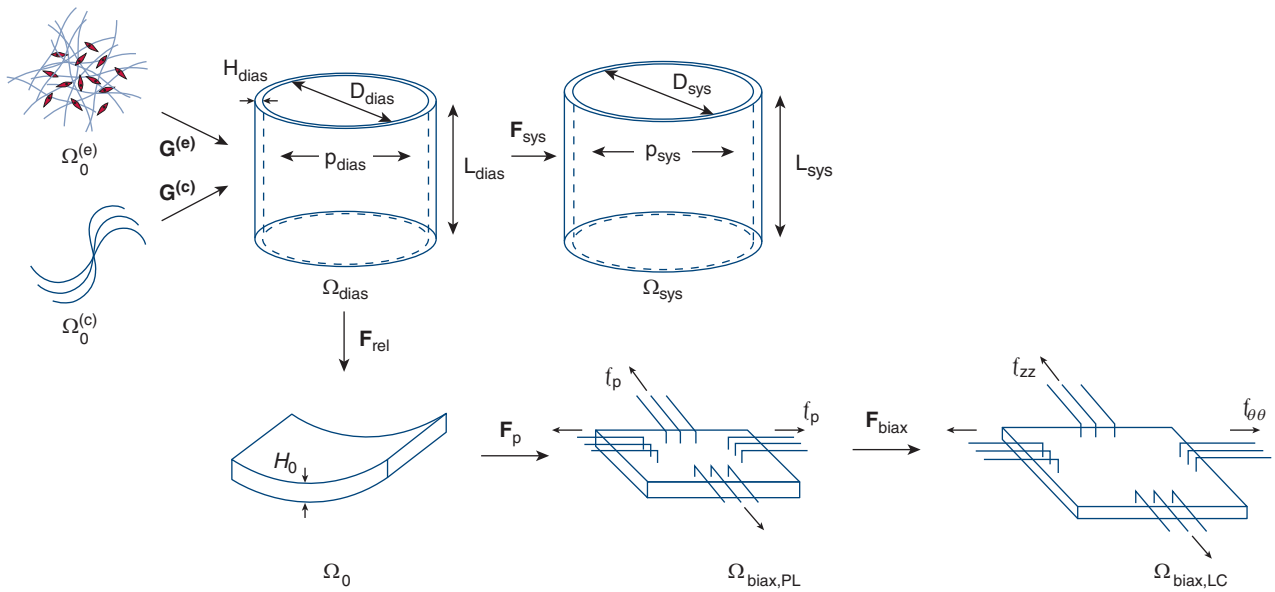


FIGURE E1. Different loading configurations Ω considered during the parameter fitting approach. Ω_{dias} and Ω_{sys} represent the in vivo diastolic (reference) and systolic configuration, respectively. $\Omega_0^{(e)}$ and $\Omega_0^{(c)}$ represent the individual stress-free state of the noncollagenous isotropic matrix and collagen, respectively. Ω_{rel} and Ω_{biax} represents the ex vivo zero-stress and biaxially loaded configuration, respectively. D_{dias} , aneurysm diameter at diastole; D_{sys} , aneurysm diameter at systole; p_{dias} , blood pressure at diastole; p_{sys} , blood pressure at systole. Figure partially adapted from Vander Linden and colleagues.¹⁹

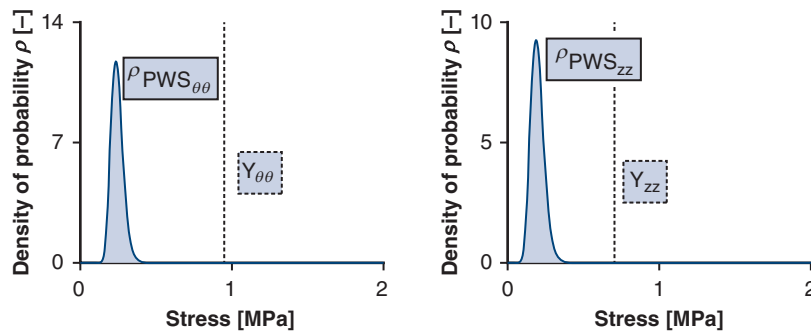


FIGURE E2. Histogram showing the PWS_{ii} values resulting from the probabilistic approach (blue) with the fitted probability density function $\rho_{PWS_{ii}}$ (solid line) and the deterministic wall strength Y_{ii} (dotted line). The corresponding probabilistic failure risk is -56.0 and -13.8 for $i=\theta$ (left) and $i=z$ (right), respectively. The results are shown for patient ATAA005. PWS , Peak wall stress.

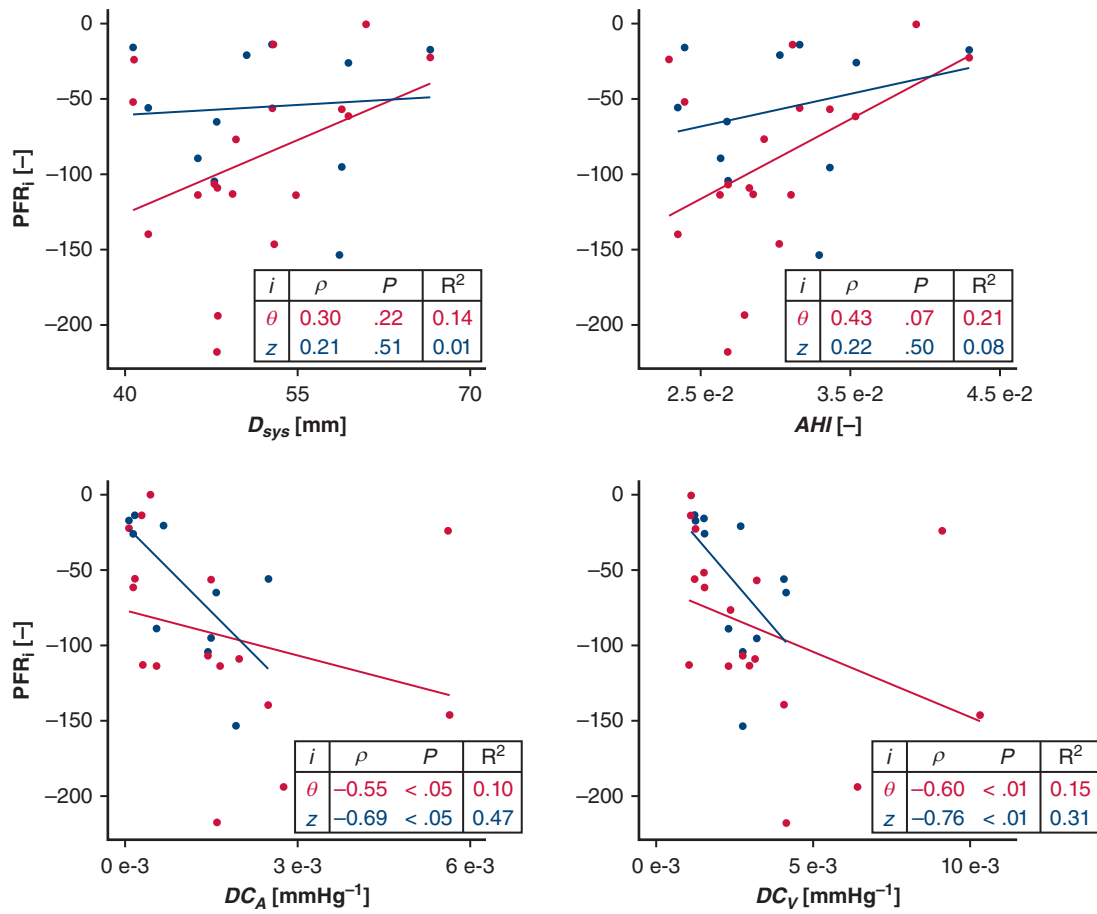


FIGURE E3. Probabilistic failure risk (PFR_i) in the circumferential (red) and axial direction (blue) with respect to D_{sys} (top left), AHI (top right), DC_A (bottom left), and DC_V (bottom right). For each of the predictors in both directions, the Spearman correlation coefficient with corresponding *P* value is given, together with the R^2 value of the linear regression. D_{sys} , Maximal aortic diameter measured at systole; AHI, aortic height index; DC_A , area-based distensibility coefficient; DC_V , volume-based distensibility coefficient.

TABLE E1. Boundaries of the material properties and in vivo thickness

Boundaries	C_{10} , kPa	k_I , kPa	k_2 , -	κ , -	α , °	H_{dias} , mm
Lower	0.5	0.5	0	0	0	$0.2 \min(H_0)_s$
Upper	7.5	50	500	1/3	90	$\min(H_0)_s$

s indicates the sample index; H_{dias} , in vivo wall thickness at diastole.

TABLE E2. Overview of the fitted parameters, fitted in vivo diastolic thickness, and fitting quality measures $NRMSE_{PB}$, $NRMSE_{H_0}$, $NRMSE_{psys}$

ATAA	H_{dias} , mm	C_{10} , kPa	k_I , kPa	k_2 , -	κ , -	α , °	$NRMSE_{PB}$, -	$NRMSE_{H_0}$, -	$NRMSE_{psys}$, -
1	2.66	2.90	820.50	165.58	0.22	57.83	0.41	0.21	9.46e-04
2	2.07	19.80	74.70	124.67	0.23	33.69	0.42	0.06	1.80e-03
3	1.73	21.40	203.40	231.31	0.22	22.37	0.24	0.08	9.08e-04
4	1.90	27.30	2.00	232.18	0.13	12.19	0.38	0.13	1.08e-03
5	1.64	19.20	91.00	71.06	0.17	33.91	0.23	0.11	8.06e-04
7	2.09	31.50	17.50	157.93	0.15	1.90	0.78	0.18	9.85e-04
8	1.70	19.90	334.50	33.92	0.17	32.94	0.23	0.17	2.14e-04
9	3.31	13.60	54.90	352.63	0.21	38.92	0.55	0.09	1.71e-04
10	2.38	14.00	128.00	68.42	0.17	30.55	0.25	0.16	9.34e-04
11	1.51	17.50	125.60	52.52	0.16	7.10	0.19	0.05	1.73e-04
12	3.03	16.00	171.10	53.85	0.20	15.78	0.55	0.08	8.90e-05
15	2.13	0.80	72.00	13.85	0.22	32.88	0.22	0.03	3.15e-04
16	2.11	14.10	296.00	77.69	0.20	33.36	0.18	0.15	5.83e-04
17	2.08	14.80	73.40	35.65	0.18	3.66	0.31	0.14	5.34e-05
18	2.48	9.10	170.10	160.73	0.21	37.87	0.26	0.13	3.55e-04
19	1.47	14.90	272.50	19.71	0.15	40.33	0.15	0.06	5.96e-04
20	1.64	12.80	81.20	33.66	0.13	3.72	0.40	0.34	5.48e-05
21	1.92	10.00	178.70	103.40	0.18	37.13	0.55	0.25	5.23e-04
22	2.08	12.00	277.40	201.60	0.23	27.00	0.29	0.13	2.76e-04
23	2.79	12.40	5.70	256.38	0.16	1.44	0.28	0.11	3.03e-04
24	1.14	8.40	456.90	4.05	0.14	43.16	0.35	0.11	2.13e-04
25	1.63	13.70	51.10	24.44	0.17	5.77	0.27	0.14	2.48e-04
26	1.26	18.20	259.50	0.72	0.16	0.29	0.26	0.16	1.49e-05
27	1.24	11.10	69.20	22.99	0.10	0.24	0.17	0.10	3.91e-04
28	1.59	16.20	434.90	25.06	0.19	35.37	0.13	0.14	2.59e-04
29	1.03	13.80	22.10	12.88	0.12	2.60	0.18	0.09	1.97e-04
30	1.73	9.30	193.20	33.38	0.17	7.56	0.25	0.16	6.12e-04
31	1.73	12.60	122.50	17.18	0.20	0.81	0.16	0.11	3.89e-05
32	1.66	15.00	372.60	34.23	0.21	0.21	0.19	0.20	4.83e-04
33	1.71	15.40	255.50	13.47	0.18	19.25	0.36	0.15	2.11e-04

$NRMSE_{PB}$, Normalized root mean squared error of the planar biaxial test results; $NRMSE_{H_0}$, normalized root mean squared error of the ex vivo thickness; $NRMSE_{psys}$, normalized root mean squared error of the systolic blood pressure; ATAA, ascending thoracic aortic aneurysm; H_{dias} , in vivo wall thickness at diastole.

TABLE E3. Spearman coefficients with corresponding *P* values of the correlation between the probabilistic failure risk *PBR*_{*i*} and clinically accessible characteristics

	Age		<i>D</i> _{sys}		<i>L</i> _{sys}		<i>V</i> _{sys}		<i>AHI</i>		<i>ASI</i>		<i>DC</i> _A		<i>DC</i> _V	
	ρ	<i>P</i>	ρ	<i>P</i>	ρ	<i>P</i>	ρ	<i>P</i>	ρ	<i>P</i>	ρ	<i>P</i>	ρ	<i>P</i>	ρ	<i>P</i>
<i>PFR</i> _{θ}	0.41	.10	0.30	.22	0.14	.59	0.36	.14	0.43	.07	0.42	.09	-0.55	.02	-0.60	.01
<i>PFR</i> _{<i>z</i>}	0.21	.51	0.21	.51	-0.24	.44	-0.04	.90	0.22	.50	0.32	.31	-0.69	.017	-0.76	.006

Significant *P* values are shown in bold. *PFR*_{*i*}, Probabilistic failure risk in the circumferential (*i*=*theta*) and axial (*i*=*z*) direction; *D*_{sys}, maximal aortic diameter measured at systole; *L*_{sys}, axial length of the aneurysm at systole; *V*_{sys}, aneurysm volume systole; *AHI*, aortic height index; *ASI*, aortic size index; *DC*_A, area-based distensibility coefficient; *DC*_V, volume-based distensibility coefficient.